



Zirconium alloyed tungsten borides synthesized by spark plasma sintering

Dariusz Garbiec¹ · Maria Wiśniewska¹ · Rafał Psiuk² · Piotr Denis² · Neonila Levintant-Zayonts² · Volf Leshchynsky¹ · Rafał Rubach¹ · Tomasz Mościcki²

Received: 13 October 2020 / Revised: 8 January 2021 / Accepted: 26 January 2021
© The Author(s) 2021

Abstract

Tungsten borides (WB_x ; $x=2.5$ or 4.5) with an increasing substitution of tungsten by zirconium from 0 to 24 at.% were synthesized by spark plasma sintering (SPS) for the first time. The influence of the holding time (2.5–30 min) on the densification behavior, microstructure evolution and development of the properties of W–Zr–B compounds were studied. The samples were characterized using scanning electron microscopy (SEM) for microstructure analysis, X-ray diffraction (XRD) for phase identification, Vickers micro-indentation for microhardness measurements, tribological tests to determine the coefficient of friction and specific wear rate, as well as measurements of electrical conductivity. The XRD results confirm the presence of the WB_4 phase in the microstructure, despite the high sintering temperature (1800 °C) and small overstoichiometric excess of boron (4.5) addition in the sintered samples. This is caused by the high heating rate (400 °C/min), short holding time (2.5 min) and addition of zirconium. The Vickers hardness (HV) values measured at 1 N are 24.8 ± 2.0 and 26.6 ± 1.8 GPa for 24 at.% zirconium in $WB_{2.5}$ and for 0 at.% zirconium in $WB_{4.5}$, respectively. In addition, the hardest sample ($W_{0.76}Zr_{0.24}B_{2.5}$) showed electrical conductivity up to $3.961 \cdot 10^6$ S/m, which is similar to WC–Co cemented carbides. The friction and wear test results reveal the formation of a boron-based film which seems to play the role of a solid lubricant.

1 Introduction

Transition-metal borides have increasingly gained scientific interest because they have high values of hardness, chemical inertness and electrical conductivity [1]. Unique properties such as the high-temperature superconductivity of magnesium diboride (MgB_2) [2], super hardness of rhenium diboride (ReB_2) [3] or high melting point of zirconium diboride (ZrB_2) [4] inspire research on new materials. Even in the form of thin films, transition-metal borides preserve their properties [5]. All of these attributes are desirable in materials for structural and engineering compounds, and could indicate that borides may be suitable replacements

for currently used carbides or nitrides in next generation cutting tools or work as refractory materials.

Among transition-metal borides, tungsten borides are a very promising group for industrial applications such as abrasive, corrosion resistant and electrode materials exposed to harsh environments [6]. Tungsten tetraboride (WB_4) is an example because of the combination of high electron density of transition metals with short covalent boron–boron bonds, this material belongs to the new generation of intrinsically superhard materials. The WB_4 microhardness value reported by Gu et al. [7] at the load of 0.49 N reached 46 GPa. WB_4 can attain an even higher hardness through the formation of solid solutions, in which the addition of an alloying element impedes dislocation motion throughout the crystal lattice [8]. The addition of zirconium caused, for example, the hardness of $W_{0.92}Zr_{0.08}B_4$ to be 34.70 ± 0.65 GPa under the applied load of 4.9 N, which is the highest value obtained for any superhard alloy at a relatively high load [8]. It should be noted that this hardness is load dependent and under the lower load (0.49 N), $W_{0.92}Zr_{0.08}B_4$ was superhard with the hardness of 55.9 ± 2.7 GPa [8]. This work is the only one in which tungsten borides with a small amount of zirconium and higher content of boron were investigated. The problem

✉ Dariusz Garbiec
dariusz.garbiec@inop.lukasiewicz.gov.pl

✉ Tomasz Mościcki
tmosc@ippt.pan.pl

¹ Łukasiewicz Research Network – Metal Forming Institute, 14 Jana Pawła II St, 61-139 Poznań, Poland

² Institute of Fundamental Technological Research Polish Academy of Sciences, 5B Pawłowskiego St, 02-106 Warsaw, Poland

is that the formation of such a structure requires molar ratios of tungsten to boron of 1:12 to prevent the formation of secondary boride phases of tungsten (e.g., WB_2) during arc-melting synthesis. Because ZrB_2 has been widely considered a potential candidate for aerospace and propulsion applications, this diboride has been doped with tungsten to improve its mechanical properties and oxidation resistance [9–11]. Hirota et al. [9] investigated the effect of ZrB_2 doping with tungsten ($Zr_{1-x}W_xB_2$; $0 < x \leq 0.5$) on the mechanical properties and thermal stability of materials obtained by the spark plasma sintering (SPS) technique. In comparison to pure ZrB_2 , the obtained materials possess much better bending strength, Vickers hardness and fracture toughness at both ambient and high temperatures. The reported high-temperature strength values exceeding 600 MPa were obtained in a test conducted at the temperature of 1600 °C [9] and more than 800 MPa at 1800 °C [4]. In addition to improvement in the mechanical properties, it has also been shown that a small addition of tungsten can result in increased resistance to oxidation at temperatures above 1500 °C due to the formation of a solid solution of $(Zr,W)B_2$ [10, 11]. Tungsten additives can also affect the densification behavior of ZrB_2 . An addition of 5 wt% tungsten caused an increase in linear shrinkage by 50% in comparison with pure ZrB_2 [12]. Kislyi et al. [12] also showed that tungsten additions of up to 10 wt% could be incorporated into a ZrB_2 solid solution. Because of the valence difference, the addition of tungsten caused the formation of vacancies, which improved densification by lowering the activation energy for sintering. While the $Zr_{1-x}W_xB_2$ ($0 < x \leq 0.5$) is quite well researched, there is not enough information about the lower content of zirconium in the WB_2 matrix. It is known that W_2B_5 and ZrB_2 form a eutectic at 20 mol% ZrB_2 with a melting point of 2180 °C [13]. Ordan'yan et al. [13] also showed that the hardness and lattice parameters practically do not differ in the whole solid solution W_2B_5 – ZrB_2 system. As was shown in [9], this conclusion is not true for solid solutions of $Zr_{1-x}W_xB_2$ ($0 < x \leq 0.12$). In this range of tungsten content, lattice parameters a and c change from 3.16 to 3.13 Å and from 3.17 to 3.15 Å, respectively, and the hardness increases from 14.1 to 20.7 GPa. It is suggested that similar situations would occur with lower contents of zirconium. Taking into account previous studies on zirconium-doped tungsten tetraboride [8] and the superhard quality of $(W,Ti)B_2$ films deposited by magnetron sputtering (MS) [14] or hybrid PLD-MS [15] with a small addition of titanium, which is in the same group of the periodic table as zirconium and builds a hexagonal structure, studies on borides with a small admixture of zirconium and low content of boron are needed. The differences of the obtained material properties may result from the used method of synthesis. Ordan'yan et al. [13] performed pre-sintering at 2000 °C and then the sample was melted via levitation melting. Hirota et al. [9]

used pulsed electric current pressure sintering (PECPS) at 1800 °C for 10 min under 30 MPa in vacuum. In this case, the samples were not melted. The change in the sintering temperature, compacting pressure and holding time are key parameters that influenced the microstructure evolution and development of properties of the obtained materials. The SPS technique provides an opportunity to investigate the influence of these parameters on the densification behavior and microstructure formation [16]. The aim of this work is to investigate the effect of the holding time as well as the influence of a low zirconium content and boron excess on density, microstructure, phase composition, mechanical properties and electrical conductivity of $W_{1-x}Zr_xB_{2.5}$ and $W_{1-x}Zr_xB_{4.5}$ ($0 < x \leq 0.24$) samples obtained by the SPS technique.

2 Materials and methods

2.1 Spark plasma sintering

Tungsten (purity: 99.9%, APS: 25 µm), zirconium (purity: 99.8%, APS: 250–350 µm) and amorphous boron (purity: 95%, APS: 1 µm) powders were mixed for 30 min using a Turbula® T2F shaker-mixer (WAB, Switzerland) in the compositions presented in Table 1. The obtained powder mixtures were SPSed in vacuum using an HP D 25/3 (FCT Systeme, Germany) furnace. The SPS process parameters are listed in Table 2. Samples with a diameter of 25.4 mm and thickness of approx. 3.5 mm were produced.

2.2 Characterization

The density of the SPSed samples was measured using the Archimedes method according to the ISO 18754:2013 standard using an EX 2225DM (Ohaus, Switzerland) scale. The phase composition of the samples was examined by XRD with a D8 Discover (Bruker, USA) using CuK_α radiation ($\lambda = 1.5418$ Å). Microscopic observations of the

Table 1 Weight content of tungsten, zirconium and boron in W/B and W/Zr/B powder mixtures

Material composition	Tungsten, g	Zirconium, g	Boron, g
$WB_{4.5}$	11.067	–	2.931
$W_{0.92}Zr_{0.08}B_{4.5}$	10.517	0.454	3.028
$W_{0.84}Zr_{0.16}B_{4.5}$	9.929	0.938	3.131
$W_{0.76}Zr_{0.24}B_{4.5}$	9.300	1.457	3.241
$WB_{2.5}$	12.202	–	1.795
$W_{0.92}Zr_{0.08}B_{2.5}$	11.635	0.502	1.861
$W_{0.84}Zr_{0.16}B_{2.5}$	11.025	1.042	1.931
$W_{0.76}Zr_{0.24}B_{2.5}$	10.366	1.624	2.007

Table 2 Spark plasma sintering process parameters of W/B and W/Zr/B powder mixtures

Material composition	Sintering temperature, °C	Heating rate, °C/min	Holding time, min	Compacting pressure, MPa
WB _{4.5}	1800	400	24	50
W _{0.92} Zr _{0.08} B _{4.5}	1800	400	2.5, 8, 15.5, 24, 30	50
W _{0.84} Zr _{0.16} B _{4.5}	1800	400	24	50
W _{0.76} Zr _{0.24} B _{4.5}	1800	400	24	50
WB _{2.5}	1800	400	24	50
W _{0.92} Zr _{0.08} B _{2.5}	1800	400	10, 24	50
W _{0.84} Zr _{0.16} B _{2.5}	1800	400	15, 24	50
W _{0.76} Zr _{0.24} B _{2.5}	1800	400	24, 30	50

microstructure and elemental microanalysis to study the elemental distribution of tungsten, zirconium and boron in the investigated samples were performed using a JSM-6010PLUS/LV (JEOL, Japan) scanning electron microscope (SEM). Energy-dispersive X-ray spectroscopy (EDS) microanalysis was used to study the distribution of elements. During the EDS measurements, the accelerating voltage of 10 kV was used. The surface topography of worn samples after wear tests was examined using an Inspect S (FEI, USA) SEM. Vickers microhardness measurements were performed using a Micro Indenter (CSM Instruments, USA). In the majority of the micro-indentation tests reported in the literature, sharp indenters (Vickers) were employed and the microhardness was specified by means of the Oliver–Pharr method [17] using a Vickers tip with the load of 1 N. Over 10 indentations on each sample were performed. The electrical conductivity was measured according to the ASTM E1004 standard using a SigmaCheck (Ether NDE, UK) eddy current conductivity meter. The wear behavior of the samples was evaluated by ball-on-disk wear tests using a T-21 (ITEE, Poland) tester. According to this method, the sliding contact is created by pushing a ball onto a rotating disc sample under a constant load. Disks 25.4 mm in diameter and 3 mm thickness and an Al₂O₃ ball of 10 mm in diameter were used at the sliding speed of 5 m/min. During the wear tests, the coefficient of friction of the tribology pair was measured in a stabilized stage of friction (after start-up), and the specific wear rate (SWR) was calculated based on the determined wear volume in accordance with Lancaster's Eq. (1) [18] shown below.

$$SWR = \frac{VL}{F \cdot SD}, \quad (1)$$

where VL (in mm³) is the disc volume loss, F (in N) is the normal load, and SD (in m) is the sliding distance. The tests were carried out without lubricant according to the ISO 2808:2004(E) standard.

3 Results and discussion

3.1 Effect of spark plasma sintering parameters on densification

The densification behavior of the powder mixtures during the SPS process, shown in Fig. 1, was analyzed based on the punch displacement dependences on the holding time. In Fig. 1a, it is clearly seen that sintering W_{0.92}Zr_{0.08}B_{4.5} for 2.5 min is not enough to complete the densification process. The minimum time required to do this is 8 min and a couple of seconds before this time, the plateau of the sintering curves is seen. It means that sintering is completed under certain conditions. Nevertheless, a further increase in the holding time (up to 15.5 min) resulted in further punch movement. This is related to the reactive sintering and partially started phase transformation from low-density hexagonal WB₄ (8.40 g/cm³ [1]) to high-density hexagonal WB₂ (12.76 g/cm³ [1]) and B phases resulted in an increase in the density of the sintered body and finished between 14–15 min without any further densification (plateau of curves). The further WB₄–WB₂ phase transformation started between 19 and 20 min and finished a couple of seconds before 24 min. Increasing the holding time to 30 min does not cause any further phase transformations or densification of the samples. The same densification behavior is observed in Fig. 1b where various powder mixtures were SPSed at the holding time of 24 min. What is clearly seen, the densification of the W_{1-x}Zr_xB_{2.5} (0 < x ≤ 0.24) was completed earlier than W_{1-x}Zr_xB_{4.5} (0 < x ≤ 0.24), which results in a lower amount of boron powder in the powder mixtures.

Changes in the density of the SPSed samples are shown in Fig. 2. It is clearly seen in Fig. 1a that as the holding time increased, the density increased and this is related to the phase transformation occurring during the holding time from the WB₄–WB₂ phase, whose density is higher than the WB₄ phase. In turn, the density of the W_{1-x}Zr_xB_{2.5} and W_{1-x}Zr_xB_{4.5} (0 < x ≤ 0.24) samples SPSed at 24 min decreases with an increasing zirconium content. The samples

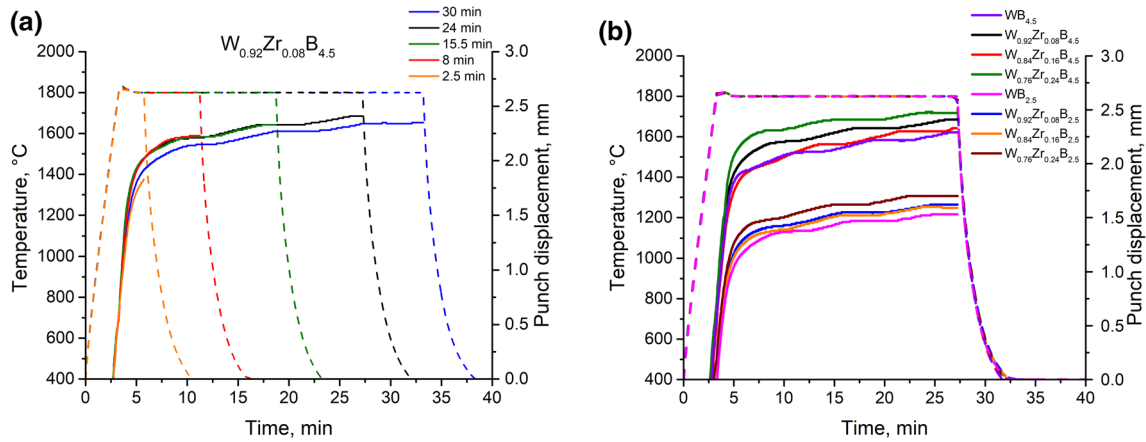


Fig. 1 Sintering curves of **a** $W_{0.92}Zr_{0.08}B_{4.5}$ samples spark plasma sintered at various holding times and **b** $W_{1-x}Zr_xB_{2.5}$ and $W_{1-x}Zr_xB_{4.5}$ ($0 < x \leq 0.24$) samples spark plasma sintered for 24 min

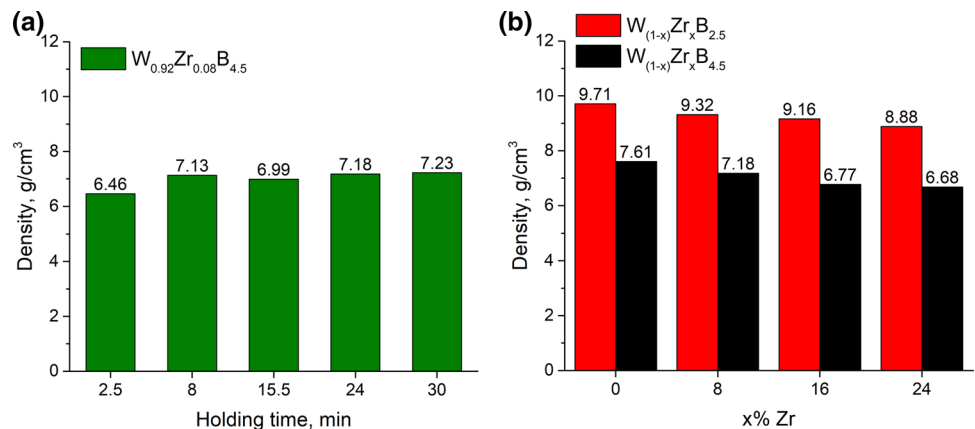
with the lower boron content have a higher density than the samples with the higher boron content and this is due to the low density of boron (2.34 g/cm^3) compared to density of tungsten (19.25 g/cm^3) and zirconium (6.51 g/cm^3).

3.2 Microstructure evolution

In Fig. 3, the distribution of elements is presented. As an exemplary, representative sample, $W_{0.84}Zr_{0.16}B_{4.5}$ with the holding time of 24 min was chosen. In Fig. 3a (SEM–BSE), the distributions of individual phases are indicated by red arrows. Due to the fact that boron is the lightest, it is visible as black fields. The tungsten compounds are the heaviest, which means that they are visible as the brightest fields. The intermediate color—light gray—is zirconium or ZrB_2 . The area of EDS analysis showed that the center of the grain mainly consists of unreacted zirconium. However, during

the SPS process, reactions take place, which result in the formation of ZrB_2 at the zirconium grain boundaries (Fig. 3b and c). The areas where tungsten is present (Fig. 3d) are characterized by different colors. As the amount of tungsten decreases, the amount of boron increases (Fig. 3c), which may indicate the presence of various tungsten borides (WB_x ; $x=2$ or 4). At the same time, in areas with the highest tungsten content, an increase in the amount of oxygen (Fig. 3f) can also be observed. Due to the high temperature and extension of the time, the amount of tungsten oxides increases. Habainy et al. [19] showed that for the time of 24 min at $907 \text{ }^\circ\text{C}$ and an atmosphere with $0.5\% \text{ O}_2$, the amount of tungsten oxides is about 3 times greater than for the time of 8 min. Increasing of the amount of WO_2 crystalline phase results in the appearance of reflections in the X-ray diffraction pattern. The black areas (Fig. 3a) are places with a high boron content. However, they do not match the oxygen distribution. It can be concluded that during the SPS process, no significant amounts of boron oxide are formed.

Fig. 2 Density of **a** $W_{0.92}Zr_{0.08}B_{4.5}$ samples spark plasma sintered at various holding times and **b** $W_{1-x}Zr_xB_{2.5}$ and $W_{1-x}Zr_xB_{4.5}$ ($0 < x \leq 0.24$) samples spark plasma sintered for 24 min



grains up to 100 μm in diameter are formed, especially when an overstoichiometric amount of boron (4.5) is used. Clusters of ZrB_2 are also evident. Their grains reach sizes around 100–200 μm . Figure 5 shows the dependences of the microstructure on the change in zirconium content in the sample after 24 min of holding time. As can be seen, the growth of zirconium content caused increases in the number of ZrB_2 grains. In the case of $\text{W}_{0.92}\text{Zr}_{0.08}\text{B}_{4.5}$ (Fig. 5c), the number of ZrB_2 grains is relatively small, which may be related to zirconium filling the vacancies in the WB_x hexagonal structure. According to Akopov et al. [8], zirconium can form a solid solution with WB_4 to a value 10 at.%. After exceeding the solubility limit, two phases— WB_2 and ZrB_2 —appear, which is confirmed by the microstructure in Fig. 5c and d. At the same time,

increasing the zirconium content reduces the amount and size of boron grains.

A similar phenomenon is observed for $\text{W}_{1-x}\text{Zr}_x\text{B}_{2.5}$ (Fig. 6). Due to the lower content of boron and also zirconium addition, the size of the boron grains decreases below 25 μm . In the case of the lower boron content, an inverse trend in the properties can be observed compared to the samples with the higher boron content. The compatibility of the material increases with increasing the zirconium content, which also results in increased microhardness and electrical conductivity.

In Fig. 7, the X-ray diffraction patterns of the $\text{W}_{1-x}\text{Zr}_x\text{B}_{4.5}$ ($0 < x \leq 0.24$) samples are presented. Despite using 4.5 atoms of boron, after 24 min of holding time, the main phase is WB_2 . The lattice parameters of this phase practically do not differ in the whole range of zirconium content from $x = 0$ to

Fig. 4 Dependence of $\text{W}_{0.92}\text{Zr}_{0.08}\text{B}_{4.5}$ microstructure on holding time. SEM–BSE micrographs spark plasma sintered for **a** 2.5, **b** 8, **c** 15.5, **d** 24 and **e** 30 min. Phases: WB_x (light gray), ZrB_2 (dark gray) and boron (black)

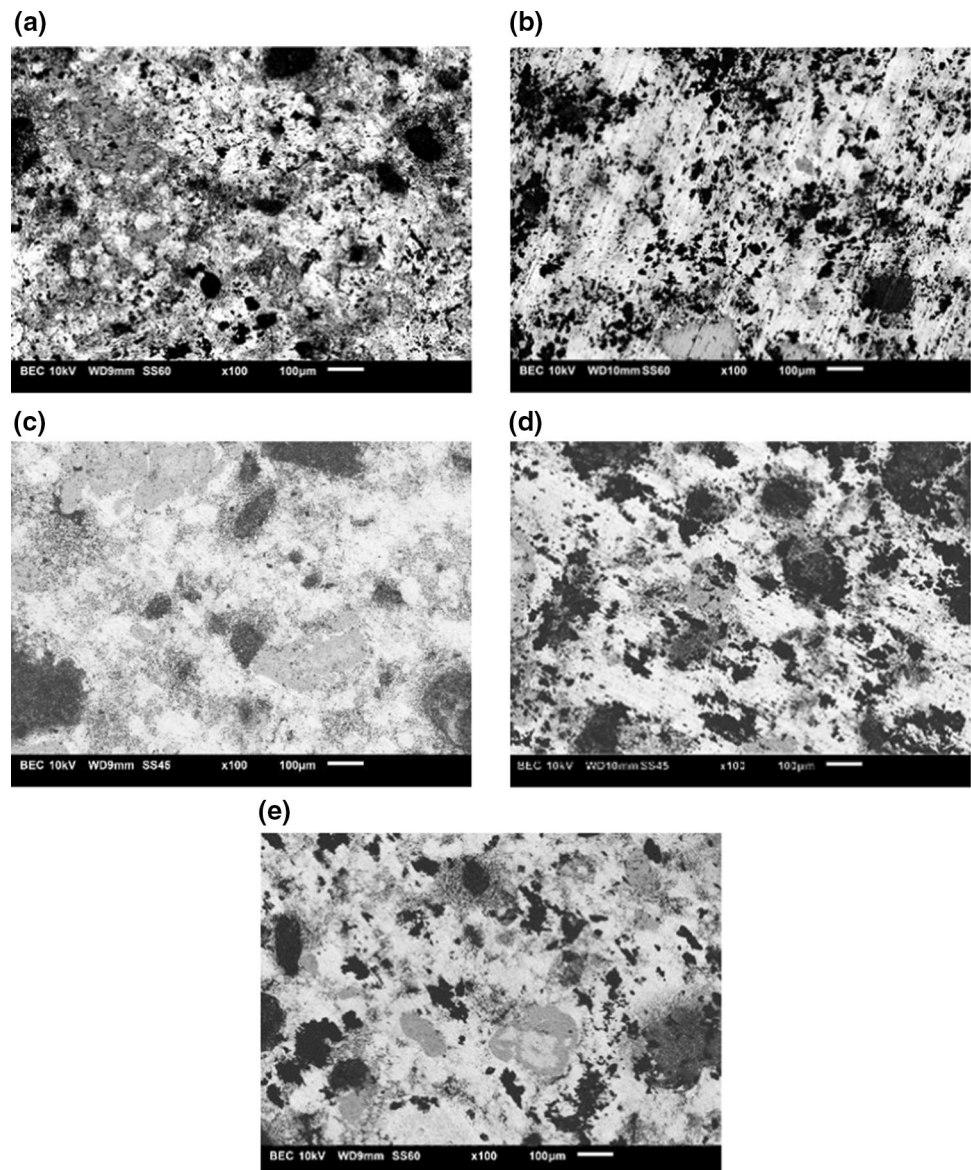


Fig. 5 Influence of zirconium alloying of $W_{1-x}Zr_xB_{4.5}$. SEM–BSE micrographs for zirconium content: **a** $x=0$, **b** $x=0.08$, **c** $x=0.16$ and **d** $x=0.24$. Holding time 24 min

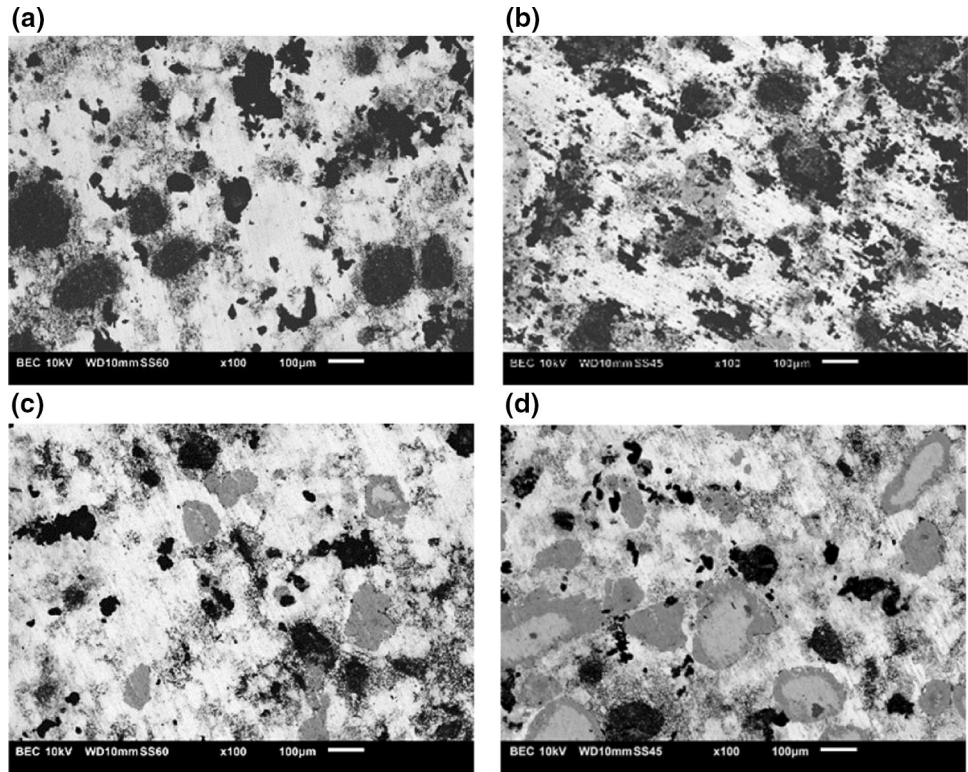
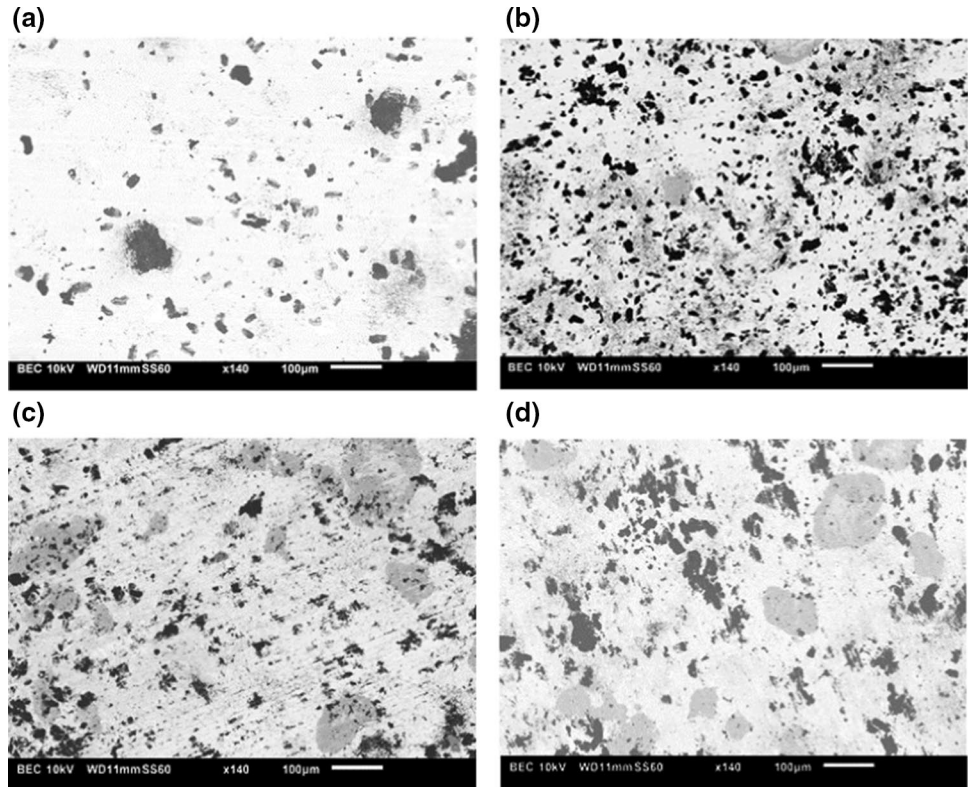


Fig. 6 Influence of zirconium alloying of $W_{1-x}Zr_xB_{2.5}$. SEM–BSE micrographs for zirconium content: **a** $x=0$, **b** $x=0.08$, **c** $x=0.16$ and **d** $x=0.24$. Holding time is 24 min



24 at.%. Parameters a and c are 2.985 and 13.900 Å, respectively, for the WB_2 phase. Similar values of those parameters were reported by Ordan'yan et al. [13] in a similar comparable W_2B_5 – ZrB_2 system. In the case of WB_4 , the a parameter is 5.202 Å and c is 6.370 Å, which is in good agreement with the data presented by Akopow et al. [1] The addition of zirconium caused the formation of hexagonal ZrB_2 (P6/mmm). Additionally, with an increasing of content of zirconium the second phase of WB_4 appears. It is a new observation because previous experimental studies [6, 20]

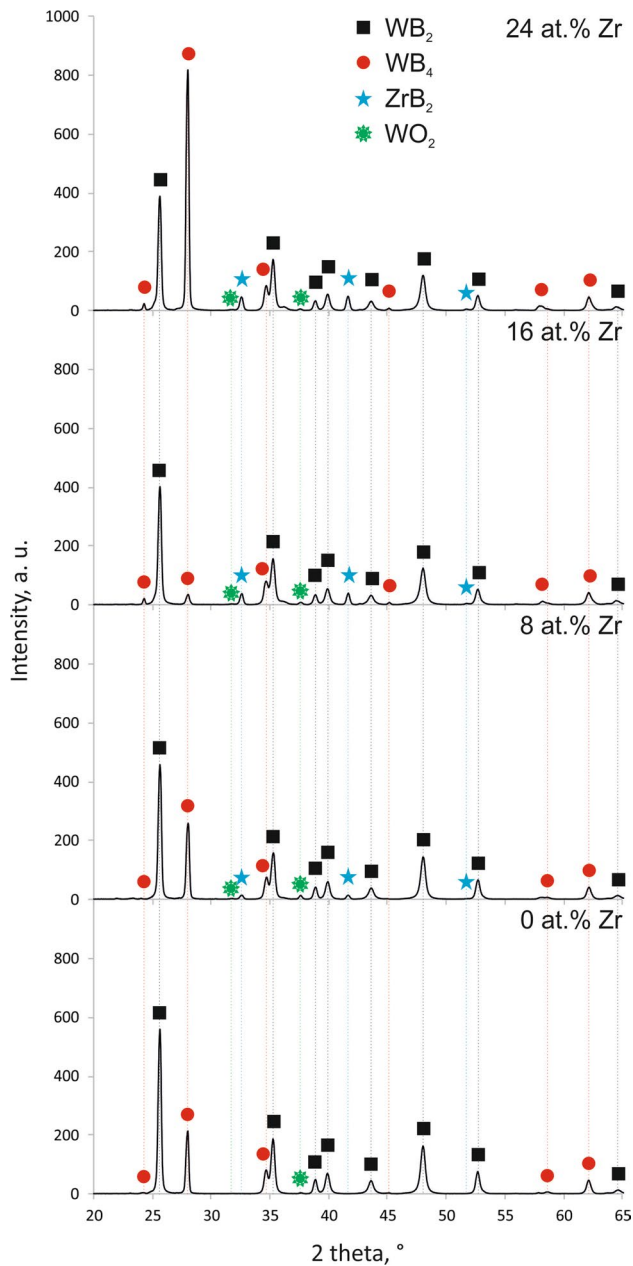


Fig. 7 XRD pattern of phase composition of samples with molar zirconium content $x=0, 8, 16$ and 24 at.% spark plasma sintered for 24 min and $B/(W+Zr)$ molar ratio of 4.5

show that metastable WB_4 decomposes into WB_2 at temperatures higher than 1600 °C. What is more, the moderate B/W molar ratio of 8 is the critical factor for the synthesis of WB_4 . As it is seen from Fig. 6, the addition of a second compound with a higher thermal stability (ZrB_2) can also increase the content of WB_4 , even if the sintering temperature is above critical (1800 °C) and the molar ratio is close to stoichiometric (4.5). Figure 6 also shows the XRD pattern of the sample without zirconium. This result confirms earlier observations [6, 20]. The XRD spectrum of the sample sintered at 1800 °C and compacting pressure of 50 MPa corresponds to the pure WB_2 phase according to the Joint Committee on Powder Diffraction and Standards (PDF No. 00-043-1386). For a zirconium content $x=0.16$ and 0.24 , there was partial decomposition from WB_2 to WB_4 .

The low content of WB_4 is detected in the samples at 2θ values of 24.3° , 33.4° and 45.1° , which correspond to the (101), (110) and (112) facets, respectively, according to the Joint Committee on Powder Diffraction and Standards (PDF No. 00-019-1373) for WB_4 . The origin of the presence of WB_4 is connected with the creation of the hexagonal ZrB_2 phase. Already at $x=8$ at.%, characteristic peaks of ZrB_2 at 2θ values of 25.1° , 32.5° , 41.5° and 57.9° are present. Zirconium forms a very favorable, stable ZrB_2 phase [13] and does not readily alloy with WB_2 or WB_4 . However, ZrB_2 can stabilize and stimulate the growth of the hexagonal crystal structure of WB_4 when a higher content of zirconium is present ($x>8$ at.%). It can be concluded that ZrB_2 precipitates first from the sintered powder mixture and provides a template pattern for further precipitation of the WB_4 phase. This phenomenon is known as precipitation hardening. Although an excessive synthesizing temperature can result in the decomposition of WB_4 [6, 20, 21], an increase in the content of zirconium can improve the crystallinity of the tungsten tetraboride phase. As presented in Fig. 8, the content of the WB_4 phase increases with shortening of the holding time.

After sintering at the holding time of 2.5 min, the strong peaks at characteristic 2θ values for WB_4 (the Joint Committee on Powder Diffraction and Standards; PDF No. 00-019-1373) are present. After increasing the holding time to 8 min, the intensity of the WB_4 peaks grow, and the content of this crystalline phase is higher than that after 2.5 min. Further extension of the holding time to 15.5 min causes the first stage of reactive sintering (Fig. 4a). The metastable WB_4 phase decomposes to the more stable WB_2 , which causes the intensity of the WB_4 peaks to diminish. Between 18 and 24 min, the second reactive sintering stage is present and the WB_4 phase practically disappears (Fig. 8). Similar observations were presented by Itoh et al. [20] for a comparable molar ratio of boron to tungsten $B/W=4.0$. A rapid increase in the amount of WB_4 was observed up to 15 min [20]. The formation of WB_4 by boron diffusion into the core of the tungsten particle prevails in the initial stage

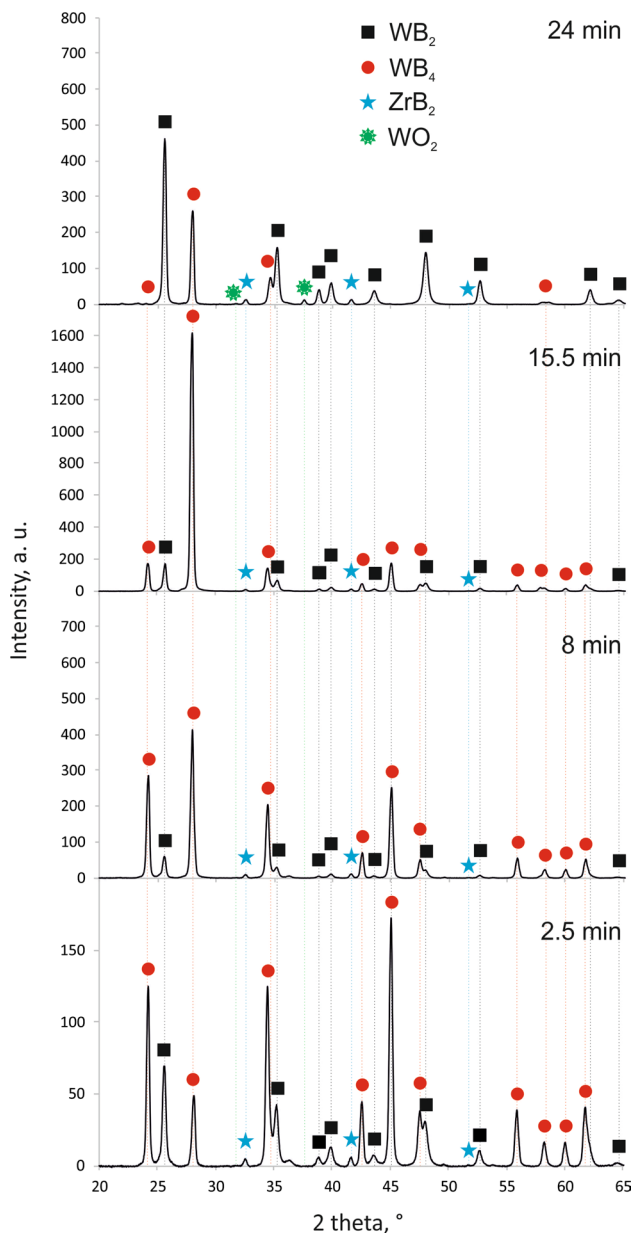


Fig. 8 XRD pattern of phase composition of samples with molar zirconium content $x=8$ at.% spark plasma sintered at various holding time and $B/(W+Zr)$ molar ratio of 4.5

of treatment due to the high concentration gradient. After 15 min, there is little punch movement (Fig. 4) and the concentration of WB_4 does not change. The system strives for equilibrium and the phase stability of WB_4 decreases due to the high sintering temperature and holding time, allowing further boron diffusion. The addition of zirconium results in the stabilization of WB_4 at the temperature of 1800 °C, whilst it is only possible at 1400 °C for the unalloyed compound [20].

The decrease in the boron to metals ratio $B/(W+Zr)$ to 2.5 results in an effect that only two compounds— WB_2 and

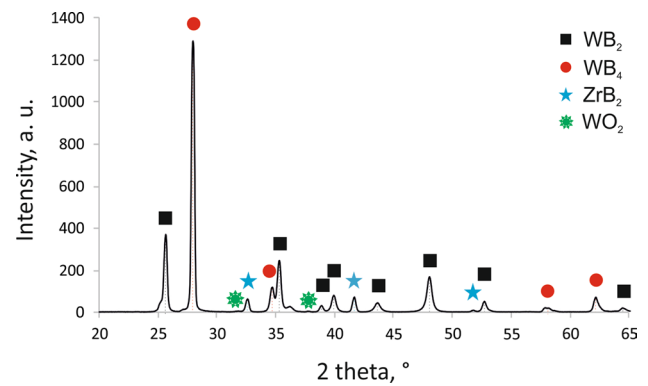


Fig. 9 XRD pattern of phase composition of sample with molar zirconium content $x=16$ at.% spark plasma sintered for 24 min and $B/(W+Zr)$ molar ratio of 2.5

ZrB_2 —are available. A variation in the holding time and also zirconium content did not influence the phase composition of the samples. The exemplary XRD pattern of the sintered materials at the temperature 1800 °C with the $B/(W+Zr)$ molar ratio of 2.5 (the molar zirconium content $x=16$ at.% and holding time 24 min) is presented in Fig. 9. The results are in agreement with the observations presented by Itoh et al. [20]. Due to the high temperature, after 24 min the amount of tungsten oxides increases. The main WO_2 peaks correspond to the 2θ positions = 26.1, 32.6 and 37.5°. Peak 26.1° lies on the slope of peak WB_2 , and therefore, it is difficult to identify. The other two can be found in the different patterns (Figs. 7, 8, 9).

3.3 Mechanical properties

In Fig. 10, the dependence of microhardness on the holding time for samples with the composition $W_{0.92}Zr_{0.08}B_{4.5}$ is presented. At the shortest holding time (2.5 min), the sample has not yet reached full densification, which results in a lower microhardness of 12.3 ± 1.3 GPa. After 8 min of sintering, the sample is fully densified under certain conditions of sintering. The sample obtains a maximum density, and thus, a maximum microhardness of 17.4 ± 2.3 GPa. In this case, the holding time is too short and despite the high temperature, the superhard WB_4 phase formed in the previous sintering stage does not decompose into $WB_2 + B$ [6]. Further sintering leads to disappearance of the WB_4 phase and its complete conversion to a softer WB_2 . Therefore, the microhardness is reduced to 11.8 ± 2.4 GPa (Fig. 11).

The addition of zirconium causes the formation of ZrB_2 and further to WB_x . Due to the fact that this compound is relatively soft, its appearance results in a decrease in the microhardness compared to the non-doped case (Fig. 11(a)).

In the case of the boron content of 4.5 (in relation to the used amount of $W+Zr$ metals) with the increase in

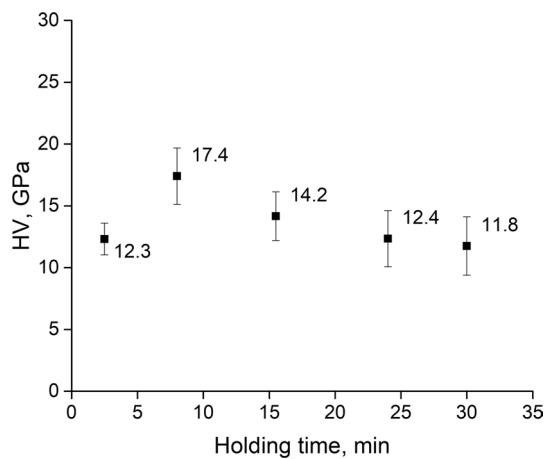


Fig. 10 Microhardness of $W_{0.92}Zr_{0.08}B_{4.5}$ samples in relation to holding time

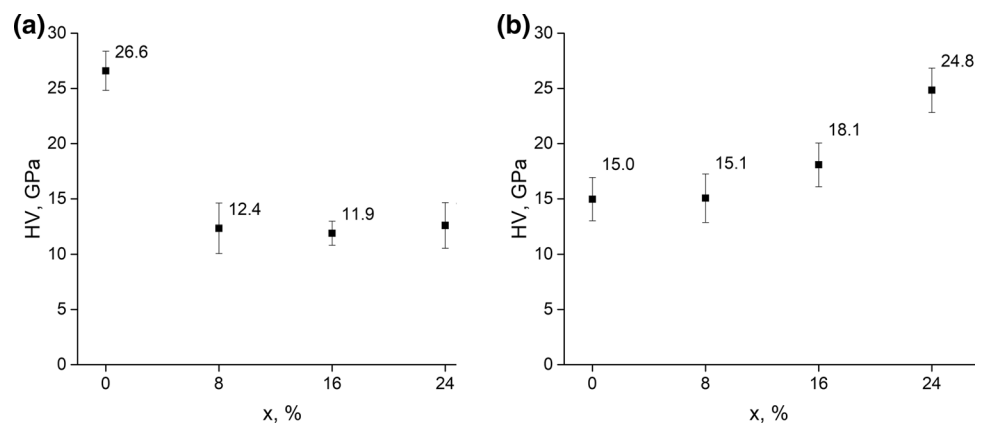
zirconium, a decrease in material densification and also a reduction in the microhardness are observed. This is due to the change in the curing mechanism from solid solution hardening to dispersive hardening. According to [22], it is indicated that zirconium is soluble in WB_4 at or below 10 at.% but at a concentration higher than 20 at.% of zirconium, the secondary phase ZrB_2 appears. Due to the smaller amount of boron (4.5 instead of 9 [8]) and the high sintering temperature, the amount of WB_4 phase is small. This can result in a change in the hardening mechanism at much lower zirconium contents. An inverse relationship can be observed for the lower boron content, where the microhardness grows with an increase in the zirconium content (Fig. 11b). As was previously shown in Fig. 8, the superhard WB_4 phase is not present under such conditions. Due to the fact that the differences in the microhardness of ZrB_2 and WB_2 at lower zirconium contents, i.e., 0 and 8 at.% are insignificant [13], this property practically does not change and is 15.1 ± 2.2 GPa (Fig. 11b). According to the phase diagram of the W_2B_5 – ZrB_2 pseudobinary system [13], a further increase in the amount of zirconium results in achieving the

composition with the lowest melting point (2180 ± 30 °C for the eutectic composition of 80 mol% W_2B_5 + 20 mol% ZrB_2). This phenomenon promotes greater densification of the material, and thus, also an increase in microhardness. Moreover, on the basis of the analysis of the microstructure of the samples with the higher zirconium content (Figs. 5 and 6), both the unbound boron and ZrB_2 grains are smaller and more evenly distributed, which promotes dispersion strengthening. A similar relationship was observed by Hirota et al. [9] when ZrB_2 was doped with small amounts of tungsten. For monolithic $Zr_{1-x}W_xB_2$ ($0 < x \leq 0.12$), W-doped ZrB_2 solid solutions with a lower hardness were formed and the hardness grew and stabilized for composites consisting of ZrB_2 solid solutions and WB_2 when $x > 0.12$ due to the formation of solid solution, homogeneously dispersed needle-like WB_2 particles [9].

The results of coefficient of friction measurements during the Al_2O_3 ball-on-disc tests are shown in Fig. 12 as the “coefficient of friction–sliding distance” diagrams and in Table 3. The diagrams demonstrate the coefficient of friction peak at the beginning of sliding and its following fall during the run-in stage. Zirconium doped tungsten borides show a coefficient of friction similar to that of non-doped tungsten borides. However, influence of the holding time on the coefficient of friction is seen (Fig. 13). The coefficient of friction decreased at the sliding distance of 300–600 m and then reached a constant value of about 0.5–0.6 (Fig. 12). The possible reason for the fall in the coefficient of friction is the formation of a “third body” [23] during sliding which consists of the particles that detached due to the wear process and formed a self-lubricating boron-based debris on the wear surface. In this case, the wear mode converts from adhesive wear to abrasive wear. One can note the minimal coefficient of friction of 0.4 is achieved for the $W_{0.76}Zr_{0.24}B_{4.5}$ sample SPSed during 24 min due to the possible solid lubrication effect of wear debris being generated during the sliding process.

The test results reveal that the specific wear rates of the investigated samples are in the range of

Fig. 11 Dependence of microhardness on the zirconium addition $x = 0$ –24 at.% for **a** $W_{1-x}Zr_xB_{4.5}$ and **b** $W_{1-x}Zr_xB_{2.5}$. Holding time is 24 min



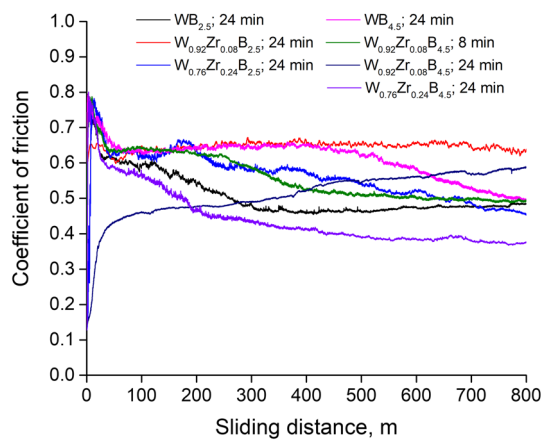


Fig. 12 Coefficient of friction diagrams of WB_{4.5}, W_{0.92}Zr_{0.08}B_{4.5} (8 min), W_{0.92}Zr_{0.08}B_{4.5}, W_{0.76}Zr_{0.24}B_{4.5}, WB_{2.5}, W_{0.92}Zr_{0.08}B_{2.5} and W_{0.76}Zr_{0.24}B_{2.5} samples spark plasma sintered for 24 min

Table 3 Coefficient of friction and specific wear rate of W_{1-x}Zr_xB_{2.5} and W_{1-x}Zr_xB_{4.5} (0 < x ≤ 0.24) samples

Material composition	Holding time, min	Coefficient of friction	Specific wear rate, mm ³ /Nm
WB _{4.5}	24	0.59	2.26 × 10 ⁻⁶
W _{0.92} Zr _{0.08} B _{4.5}	8	0.54	9.42 × 10 ⁻⁶
W _{0.92} Zr _{0.08} B _{4.5}	15.5	0.53	1.40 × 10 ⁻⁶
W _{0.92} Zr _{0.08} B _{4.5}	24	0.53	2.28 × 10 ⁻⁶
W _{0.92} Zr _{0.08} B _{4.5}	30	0.59	1.36 × 10 ⁻⁵
W _{0.84} Zr _{0.16} B _{4.5}	24	0.57	1.23 × 10 ⁻⁵
W _{0.76} Zr _{0.24} B _{4.5}	24	0.45	1.14 × 10 ⁻⁶
WB _{2.5}	24	0.50	5.77 × 10 ⁻⁶
W _{0.92} Zr _{0.08} B _{2.5}	24	0.64	1.44 × 10 ⁻⁵
W _{0.84} Zr _{0.16} B _{2.5}	24	0.55	1.05 × 10 ⁻⁵
W _{0.76} Zr _{0.24} B _{2.5}	24	0.54	3.33 × 10 ⁻⁵

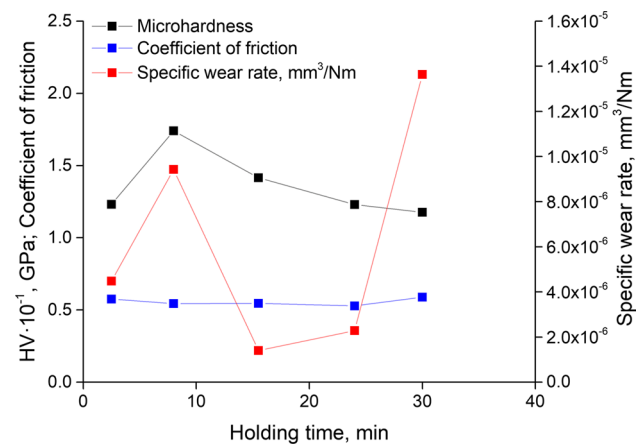
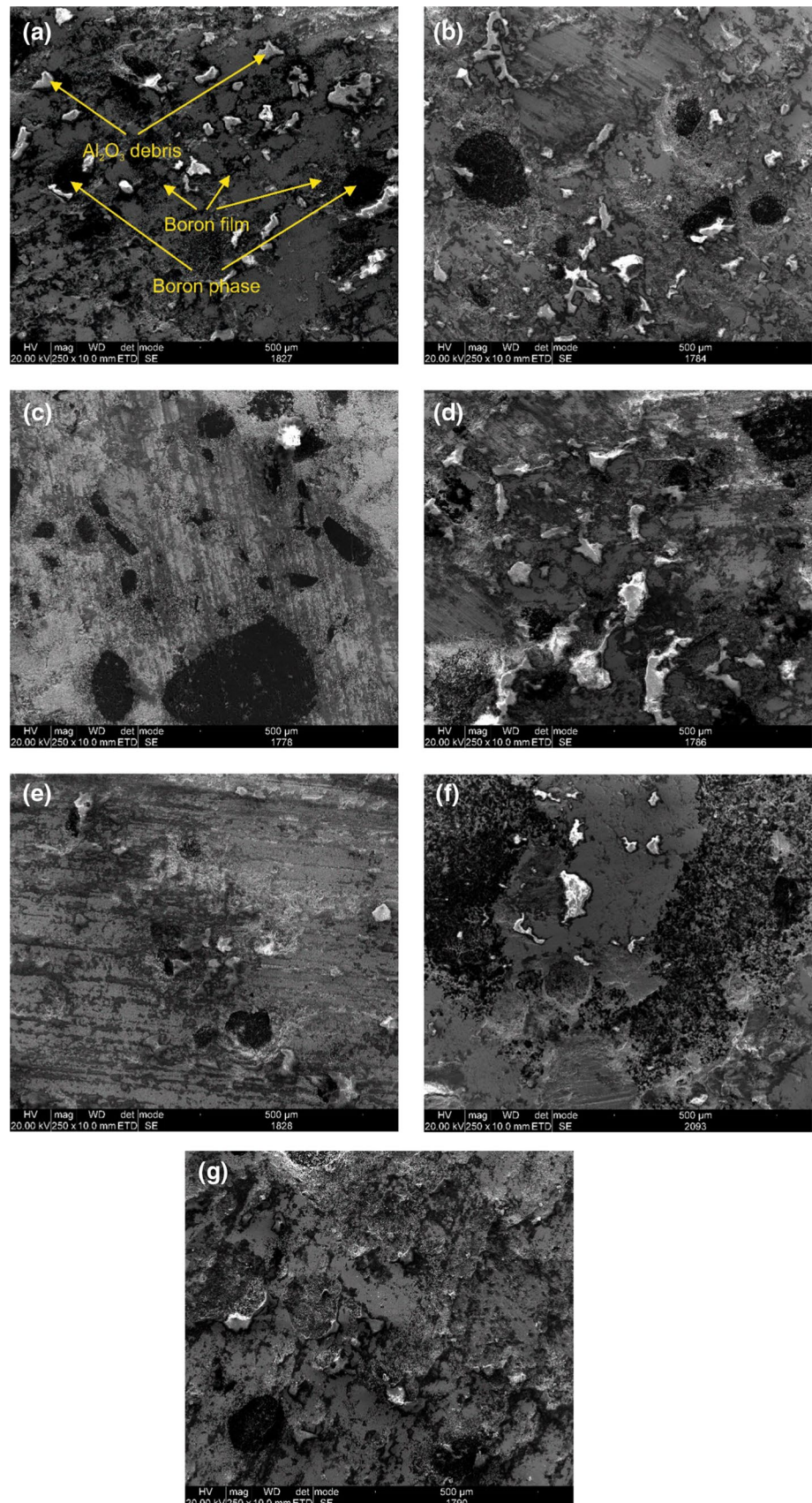


Fig. 13 Influence of holding time on properties of W_{0.92}Zr_{0.08}B_{4.5} samples spark plasma sintered at various holding times

1 × 10⁻⁶–3 × 10⁻⁵ mm³/Nm (Table 3), which is similar to those of WC–Co–Cr₃C₂–VC composites spark plasma sintered at 1100 °C for 5 min with an applied compacting pressure of 80 MPa and a heating rate of 100 °C/min [24]. The wear mechanism and the associated SWR depend critically on the sintering conditions. The wear resistance of W–Zr–B materials is assumed to be a function of the grain size, phase composition and the strength of the particle and grain boundaries similar to the wear behavior of WC–Co composites [24]. In this case, the hardness looks like the best indicator of wear resistance, and cemented carbides with their high hardness are usually more resistant. However, the WB_{4.5} and W_{0.92}Zr_{0.08}B_{4.5} samples exhibit some differences in the friction behavior—a small peak of the coefficient of friction and a larger run-in period (Fig. 12). The microhardness peak for W_{0.92}Zr_{0.08}B_{4.5} shown in Fig. 13 does not prove the high wear resistance of this material. In contrast, the highest wear resistance (minimum of SWR) is achieved at a lower microhardness. The probable reason for such behavior seems to be the lubrication effect of the wear particles at the sliding interface. One can note that the hardness of the composite in the range of 12–16 GPa is comparable and higher than that of the Al₂O₃ ball, which results in wear of the Al₂O₃ ball and an increase in the Al₂O₃ particle content in the wear debris. This effect may lead to an escalation in abrasive wear at the sliding interface as well as the presence of an SWR peak. The diminishing composite hardness due to the increase in the SPS holding time changes the wear mechanism and results in possible utilization of the solid lubrication effect due to the generation of a boron-based film. The results indicate a sharp increase in the SWR of the composites SPSed at the holding time of 30 min (Fig. 13) because of possible grain growth.

From this viewpoint, the morphology of the wear tracks formed in the zirconium-doped and non-doped tungsten borides samples after the wear tests was observed by SEM. The results shown in Fig. 14. Figure 14a demonstrate the wear track at 200× magnification without any evidence of microcracks. It is known that for conventional ceramic materials, the dominant mechanism of material removal is grain boundary fracture combined with lateral crack chipping [24]. However, brittle fracture was not observed in our case. The wear mechanism observed at the interface seems to be abrasive wear with additional lubrication in the form of a boron-based film which is clearly seen in the micrographs (black areas and arrows). This film is not seen in the areas outside of the wear track (Fig. 13a) or in micrographs Figs. 4 and 5. Only the very fine powder-like wear debris of Al₂O₃ was observed. The large and bright block-like debris, Al₂O₃ particles, are seen as evidence of Al₂O₃ ball abrasive wear (Fig. 14b and c). The boron-based film is believed to originate from the boron phase, and examination of the film

Fig. 14 Wear track of **a** $WB_{4.5}$, **b** $W_{0.92}Zr_{0.08}B_{4.5}$ (8 min), **c** $W_{0.92}Zr_{0.08}B_{4.5}$, **d** $W_{0.76}Zr_{0.24}B_{4.5}$, **e** $WB_{2.5}$, **f** $W_{0.92}Zr_{0.08}B_{2.5}$ and **g** $W_{0.76}Zr_{0.24}B_{2.5}$ samples spark plasma sintered for 24 min



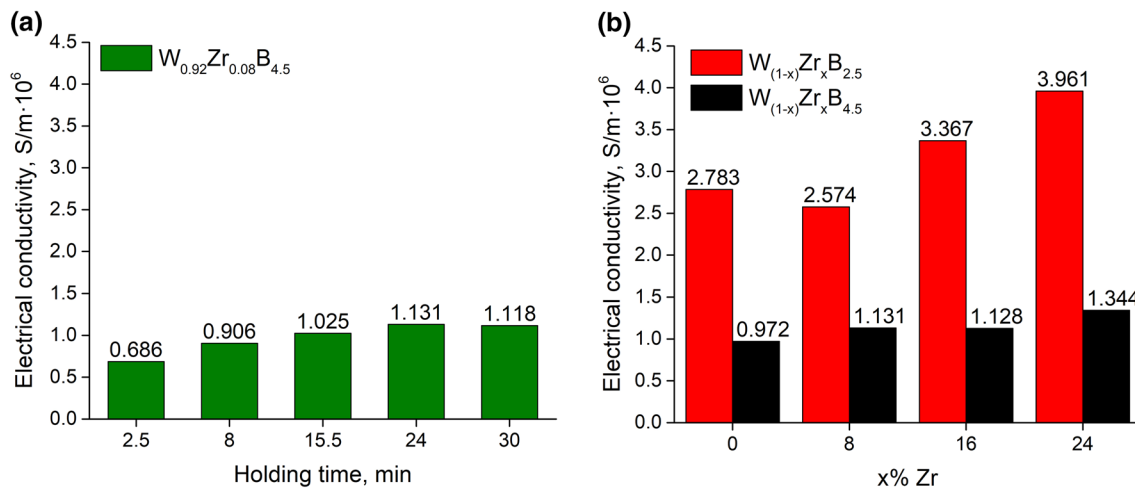


Fig. 15 Electrical conductivity of **a** $W_{0.92}Zr_{0.08}B_{4.5}$ samples spark plasma sintered at various holding times and **b** $W_{1-x}Zr_xB_{2.5}$ and $W_{1-x}Zr_xB_{4.5}$ ($0 < x \leq 0.24$) samples spark plasma sintered for 24 min

composition will be conducted in future research. The presence of the boron-based film which seems to play the role of solid lubricant demonstrates the possibility to use sintered W–Zr–B materials to make machining tools and various components working in harsh conditions.

3.4 Electrical conductivity

The electrical conductivity of the $W_{1-x}Zr_xB_{2.5}$ and $W_{1-x}Zr_xB_{4.5}$ ($0 < x \leq 0.24$) samples is shown in Fig. 15. It is clearly seen that the electrical conductivity of the samples with the lower boron content is more or less three times higher than the samples with the higher boron content and increases at ambient temperature with an increasing zirconium content up to 3.961×10^6 S/m. This is a result of the poor electrical conductivity of boron (1.0×10^{-4} S/m) [25] and better electrical conductivity of zirconium (2.4×10^6 S/m) [25]. Furthermore, the increased holding time has an influence on the electrical conductivity of the SPSed samples (example in Fig. 15b). The electrical conductivity of $W_{1-x}Zr_xB_{4.5}$ ($0 < x \leq 0.24$) increased from 0.906×10^6 S/m (holding time 8 min) to 1.131×10^6 S/m (holding time 24 min). This is a result of the increasing density of the samples with increased holding time. The electrical conductivity of $W_{1-x}Zr_xB_{2.5}$ ($0 < x \leq 0.24$) is similar to the electrical conductivity of WC–Co cemented carbides, which is 4.76×10^6 S/m [26].

4 Conclusions

In this work, samples of tungsten borides (WB_x ; $x = 2.5$ or 4.5) with an increasing substitution of tungsten by zirconium from 0 to 24 at.% were synthesized for the first time by spark plasma sintering. The influence of the process parameters, mainly the holding time (2.5–30 min), on the properties of W–Zr–B compounds was also studied. The main conclusions are:

- The boron and zirconium content influence on the densification behavior. The increase in the zirconium content caused a decrease in the density of the SPSed samples. The samples with a higher boron content are characterized by a lower density than the samples with the lower boron content and this is related to the high difference between the boron and tungsten and zirconium density.
- With an increasing holding time (> 9 min), two stages of reactive spark plasma sintering were observed, and hence WB_4 phase decomposition to $WB_2 + 2B$ occurred.
- A rapid heating rate (400 °C/min), short holding time (2.5 min), zirconium doping and small boron overstoichiometric ($B \text{ at.}/(W + Zr) \text{ at.} = 4.5$) caused the samples spark plasma sintered at the relatively high sintering temperature of 1800 °C (higher than the temperature limit of the occurring WB_4) to be characterized by a microstructure still containing the WB_4 phase.
- For $W_{1-x}Zr_xB_{4.5}$ ($0 < x \leq 0.24$) the higher content of zirconium caused a decrease in hardness from 26.6 ± 1.8 to 11.9 ± 1.1 GPa. In contrast, for $W_{1-x}Zr_xB_{2.5}$ ($0 < x \leq 0.24$) the hardness increases from 15.0 ± 2.0 to 24.8 ± 2.0 GPa.

- The SPSed samples are characterized by a specific wear rate in the range of 1×10^{-6} – 3×10^{-5} mm³/Nm. The friction and wear test results reveal the formation of a boron-based film which seems to play the role of solid lubricant. This effect demonstrates the possibility to use sintered W–Zr–B materials to make machining tools and various components working in harsh conditions.
- With an increasing zirconium content, the electrical conductivity of the SPSed samples increased both in $W_{1-x}Zr_xB_{4.5}$ and $W_{1-x}Zr_xB_{4.5}$ ($0 < x \leq 0.24$). $W_{0.76}Zr_{0.24}B_{2.5}$ sintered at a 24 min holding time has the highest electrical conductivity of 3.961×10^6 S/m, which is similar to the electrical conductivity of WC–Co cemented carbides.

The very good usable properties of the obtained materials mean that W–Zr–B compounds may in the future be competitive with currently used materials such as tungsten carbide–cobalt cemented carbides. Due to the high electrical conductivity, hardness, wear resistance and also relatively simple and fast synthesis method, the developed material can be used in many fields of industry.

Acknowledgments This work was supported by the National Science Centre (NCN, Poland), Research Project: UMO-2017/25/B/ST/8/01789.

Open Access This article is licensed under a Creative Commons Attribution 4.0 International License, which permits use, sharing, adaptation, distribution and reproduction in any medium or format, as long as you give appropriate credit to the original author(s) and the source, provide a link to the Creative Commons licence, and indicate if changes were made. The images or other third party material in this article are included in the article's Creative Commons licence, unless indicated otherwise in a credit line to the material. If material is not included in the article's Creative Commons licence and your intended use is not permitted by statutory regulation or exceeds the permitted use, you will need to obtain permission directly from the copyright holder. To view a copy of this licence, visit <http://creativecommons.org/licenses/by/4.0/>.

References

1. Akopov G, Yeung MT, Kaner RB. Rediscovering the crystal chemistry of borides. *Adv Mater.* 2017;29(21):1604506. <https://doi.org/10.1002/adma.201604506>.
2. Nagamatsu J, Nakagawa N, Muranaka T, Zenitani Y, Akimitsu J. Superconductivity at 39 K in magnesium diboride. *Nature.* 2001;410(6824):63–4. <https://doi.org/10.1038/35065039>.
3. Chung H-Y, Weinberger MB, Levine JB, Kavner A, Yang J-M, Tolbert SH, et al. Synthesis of ultra-incompressible superhard rhenium diboride at ambient pressure. *Science.* 2007;316(5823):436. <https://doi.org/10.1126/science.1139322>.
4. Silvestroni L, Kleebe H-J, Fahrenholtz WG, Watts J. Superstrong materials for temperatures exceeding 2000 °C. *Sci Rep.* 2017;7(1):40730. <https://doi.org/10.1038/srep40730>.
5. Chrzanowska-Gizyńska J, Denis P, Hoffman J, Gizyński M, Mosciński T, Garbiec D, et al. Tungsten borides layers deposited by a nanosecond laser pulse. *Surf Coat Technol.* 2018;335:181–7. <https://doi.org/10.1016/j.surfcoat.2017.12.040>.
6. Ma K, Cao X, Yang H, Xue X. Formation of metastable tungsten tetraboride by reactive hot-pressing. *Ceram Int.* 2017;43(12):8551–5. <https://doi.org/10.1016/j.ceramint.2017.03.059>.
7. Gu Q, Krauss G, Steurer W. Transition metal borides: superhard versus ultra-incompressible. *Adv Mater.* 2008;20(19):3620–6. <https://doi.org/10.1002/adma.200703025>.
8. Akopov G, Yeung MT, Turner CL, Mohammadi R, Kaner RB. Extrinsic hardening of superhard tungsten tetraboride alloys with group 4 transition metals. *J Am Chem Soc.* 2016;138(17):5714–21. <https://doi.org/10.1021/jacs.6b02676>.
9. Ken H, Endo T, Masaki K, Nakane S, Nishimura T, Morisada Y, et al. Simultaneous synthesis and consolidation of W-added ZrB₂ by pulsed electric current pressure sintering and their mechanical properties. *Mater Sci Forum.* 2007;561–565:527–30. <https://doi.org/10.4028/www.scientific.net/MSF.561-565.527>.
10. Silvestroni L, Sciti D, Monteveder F, Stricker K, Kleebe H-J. Microstructure evolution of a W-doped ZrB₂ ceramic upon high-temperature oxidation. *J Am Ceram Soc.* 2017;100(4):1760–72. <https://doi.org/10.1111/jace.14738>.
11. Jiang Y, Li R, Zhang Y, Zhao B, Li J, Feng Z. Tungsten doped ZrB₂ powder synthesized synergistically by co-precipitation and solid-state reaction methods. *Procedia Eng.* 2012;27:1679–85. <https://doi.org/10.1016/j.proeng.2011.12.636>.
12. Kislyi PS, Kuzenkova MA, Zaverukha OV. On the sintering process of zirconium diboride with tungsten. *Phys Sinter.* 1971;3:29–44.
13. Ordan'yan SS, Boldin AA, Suvorov SS, Smirnov VV. Phase diagram of the W₂B₅–ZrB₂ system. *Inorg Mater.* 2005;41(3):232–4. <https://doi.org/10.1007/s10789-005-0114-0>.
14. Mosciński T, Psiuk R, Słomińska H, Levintan-Zayonts N, Garbiec D, Pisarek M, et al. Influence of overstoichiometric boron and titanium addition on the properties of RF magnetron sputtered tungsten borides. *Surf Coat Technol.* 2020;390:125689. <https://doi.org/10.1016/j.surfcoat.2020.125689>.
15. Chrzanowska-Giżyńska J, Denis P, Giżyński M, Kurpaska Ł, Mihailescu I, Ristoscu C, et al. Thin WB_x and W_yTi_{1-y}B_x films deposited by combined magnetron sputtering and pulsed laser deposition technique. *Appl Surf Sci.* 2019;478:505–13. <https://doi.org/10.1016/j.apsusc.2019.02.006>.
16. Garbiec D, Siwak P. Study on microstructure and mechanical properties of spark plasma sintered Alumix 431 powder. *Powder Metall.* 2016;59(4):242–8. <https://doi.org/10.1080/00325899.2016.1169362>.
17. Oliver WC, Pharr GM. An improved technique for determining hardness and elastic modulus using load and displacement sensing indentation experiments. *J Mater Res.* 1992;7(6):1564–83. <https://doi.org/10.1557/JMR.1992.1564>.
18. Lancaster JK. The influence of substrate hardness on the formation and endurance of molybdenum disulphide films. *Wear.* 1967;10(2):103–17. [https://doi.org/10.1016/0043-1648\(67\)90082-8](https://doi.org/10.1016/0043-1648(67)90082-8).
19. Habainy J, Nilsson C. Oxidation of pure tungsten in the temperature interval 400–900 °C. Master's Thesis. Lund University, Lund 2013.
20. Itoh H, Matsudaira T, Naka S, Hamamoto H, Obayashi M. Formation process of tungsten borides by solid state reaction between tungsten and amorphous boron. *J Mater Sci.* 1987;22(8):2811–5. <https://doi.org/10.1007/BF01086475>.
21. Li X, Tao Y, Peng F. Pressure and temperature induced phase transition in WB₄: a first principles study. *J Alloy Compd.* 2016;687:579–85. <https://doi.org/10.1016/j.jallcom.2016.06.146>.
22. Gao Y, Gao K, Fan L, Yang F, Guo X, Zhang R, et al. Oscillatory pressure sintering of WC–Fe–Ni cemented carbides. *Ceram Int.* 2020;46(8, Part B):12727–31. <https://doi.org/10.1016/j.ceramint.2020.02.040>.

23. Bai L, Qi J, Lu Z, Zhang G, Wang L, Wang Y, et al. Theoretical study on tribological mechanism of solid lubricating films in a sand–dust environment. *Tribol Lett.* 2013;49(3):545–51. <https://doi.org/10.1007/s11249-012-0095-5>.
24. Espinosa-Fernández L, Borrell A, Salvador MD, Gutierrez-Gonzalez CF. Sliding wear behavior of WC–Co–Cr₃C₂–VC composites fabricated by conventional and non-conventional techniques. *Wear.* 2013;307(1):60–7. <https://doi.org/10.1016/j.wear.2013.08.003>.
25. <https://periodictable.com/Properties/A/ElectricalConductivity.an.html>. Accessed 1 Oct 2020
26. Guimarães B, Fernandes CM, Figueiredo D, Cerqueira MF, Carvalho O, Silva FS, et al. A novel approach to reduce in-service temperature in WC–Co cutting tools. *Ceram Int.* 2020;46(3):3002–8. <https://doi.org/10.1016/j.ceramint.2019.09.299>.

Publisher's Note Springer Nature remains neutral with regard to jurisdictional claims in published maps and institutional affiliations.